



# Marine-derived $\kappa$ -carrageenan-coated zinc oxide nanoparticles for targeted drug delivery and apoptosis induction in oral cancer

Vanitha Marunganathan<sup>1</sup> · Meenakshi Sundaram Kishore Kumar<sup>2</sup> · Zulhisyam Abdul Kari<sup>3,4</sup> · Jayant Giri<sup>5</sup> · Mohammed Rafi Shaik<sup>6</sup> · Baji Shaik<sup>7</sup> · Ajay Guru<sup>1</sup>

Received: 17 October 2023 / Accepted: 12 December 2023  
© The Author(s), under exclusive licence to Springer Nature B.V. 2024

## Abstract

**Background** *Kappaphycus alvarezii*, a marine red algae species, has gained significant attention in recent years due to its versatile bioactive compounds. Among these,  $\kappa$ -carrageenan (CR), a sulfated polysaccharide, exhibits remarkable antimicrobial properties. This study emphasizes the synergism attained by functionalizing zinc oxide nanoparticles (ZnO NPs) with CR, thereby enhancing its antimicrobial efficacy and target specificity against dental pathogens.

**Methods** In this study, we synthesized ZnO-CR NPs and characterized them using SEM, FTIR, and XRD techniques to authenticate their composition and structural attributes. Moreover, our investigation revealed that ZnO-CR NPs possess better free radical scavenging capabilities, as evidenced by their effective activity in the DPPH and ABTS assay.

**Results** The antimicrobial properties of ZnO-CR NPs were systematically assessed using a zone of inhibition assay against dental pathogens of *S. aureus*, *S. mutans*, *E. faecalis*, and *C. albicans*, demonstrating their substantial inhibitory effects at a minimal concentration of 50  $\mu\text{g/mL}$ . We elucidated the interaction between CR and the receptors of dental pathogens to further understand their mechanism of action. The ZnO-CR NPs demonstrated a dose-dependent anticancer effect at concentrations of 5  $\mu\text{g/mL}$ , 25  $\mu\text{g/mL}$ , 50  $\mu\text{g/mL}$ , and 100  $\mu\text{g/mL}$  on KB cells, a type of Human Oral Epidermal Carcinoma. The mechanism by which ZnO-CA NPs induced apoptosis in KB cells was determined by observing an increase in the expression of the BCL-2, BAX, and P53 genes.

**Conclusion** Our findings unveil the promising potential of ZnO-CR NPs as a candidate with significant utility in dental applications. The demonstrated biocompatibility, potent antioxidant and antiapoptotic activity, along with impressive antimicrobial efficacy position these NPs as a valuable resource in the ongoing fight against dental pathogens and oral cancer.

**Keywords**  $\kappa$ -carrageenan · Zinc oxide nanoparticle · Dental pathogen · Antimicrobial

✉ Ajay Guru  
ajayguru.sdc@saveetha.com

<sup>1</sup> Department of Cariology, Saveetha Dental College and Hospitals, Saveetha Institute of Medical and Technical Sciences, Saveetha University, Chennai, India

<sup>2</sup> Department of Anatomy, Biomedical Research Unit and Laboratory Animal Centre (BRULAC), Saveetha Dental College and Hospitals, Saveetha Institute of Medical and Technical Sciences, Saveetha University, Chennai 600077, India

<sup>3</sup> Department of Agricultural Sciences, Faculty of Agro-Based Industry, Universiti Malaysia Kelantan, Jeli Campus, 17600 Jeli, Malaysia

<sup>4</sup> Faculty of Agro-Based Industry, Advanced Livestock and Aquaculture Research Group, Universiti Malaysia Kelantan, Jeli Campus, 17600 Jeli, Malaysia

<sup>5</sup> Department of Mechanical Engineering, Yeshwantrao Chavan College of Engineering, Nagpur, India

<sup>6</sup> Department of Chemistry, College of Science, King Saud University, P.O. Box 2455, Riyadh 11451, Saudi Arabia

<sup>7</sup> School of Chemical Engineering, Yeungnam University, Gyeongsan 38541, Republic of Korea

## Introduction

*Kappaphycus alvarezii*, commonly known as ‘cottonii’ or ‘carrageenophyte,’ is a species of marine red algae. It contains bioactive compounds that have demonstrated potential antimicrobial and anticancer activities [1]. These compounds can inhibit the growth of certain bacteria, fungi, and even viruses. The antimicrobial properties are attributed to various secondary metabolites present in the algae, such as sulfated polysaccharides, peptides, and polyphenols [2].  $\kappa$ -Carrageenan (CR) is a natural polysaccharide derived from the cell walls of red algae, particularly from species like *Kappaphycus alvarezii* [3]. It is widely used in various industries, including food, pharmaceuticals, and cosmetics, due to its unique biological and physicochemical properties. CR has been shown to modulate the immune system, stimulating immune responses such as the activation of immune cells like macrophages and natural killer cells [4]. These immune cells play a vital role in identifying and eliminating cancer cells from the body. Apoptosis, or programmed cell death, is a natural process that helps remove damaged or unwanted cells from the body. Cancer cells often resist apoptosis, but some studies suggest that  $\kappa$ -carrageenan can induce apoptosis in cancer cells, promoting their self-destruction [5]. Against bacteria, CR operates by perturbing cell membranes and walls, provoking a release of cellular contents and ensuing cell demise. This profound disruption sabotages the integrity of bacterial cells, effectively impeding their growth [6]. Its role as a potential natural preservative in food products is founded upon this antibacterial attribute, restraining the proliferation of foodborne pathogens [7, 8]. Furthermore, CR potential extends to medical applications, where it could find use in wound dressings to mitigate bacterial infections [9]. Notably, CR antimicrobial activity extends to fungal pathogens as well. By interfering with fungal cell wall synthesis and compromising membrane integrity, it orchestrates a sequence of events that obstruct vital cellular processes and culminate in fungal cell demise. As an alternative to synthetic antifungal agents, CR could offer a more sustainable approach to combat fungal infections, spanning agricultural, medical, and personal care domains [10]. The underlying mechanisms of CR antimicrobial efficacy predominantly originate from its interactions with microbial surfaces. The sulfate groups present within CR molecules, endowed with negative charges, engage positively charged components on microbial cell surfaces. This interaction precipitates a cascade of structural disruptions, compromising essential cellular functions and culminating in the demise of the targeted microorganisms [11].

Dental pathogens encompass a range of microorganisms that establish colonization within the oral cavity,

precipitating infections that give rise to an array of dental and oral health predicaments [12]. Inadequate oral hygiene practices and the persistent inflammation of oral tissues, commonly linked to conditions such as gum disease (periodontitis) or ongoing irritation from sharp or fractured teeth, can significantly raise the risk of oral cancers, including epidermoid carcinoma. Epidermoid carcinoma can emerge within various areas of the oral cavity, encompassing the lips, tongue, gums, cheeks, and the oral lining. It often manifests as persistent ulcers or sores that resist healing, the presence of lumps or masses, or alterations in the color and texture of oral tissues [13]. In this context, we shall delve into the distinct complications attributed to prevalent dental pathogens, specifically *Staphylococcus aureus*, *Streptococcus mutans*, *Enterococcus faecalis*, and *Candida albicans*. *Staphylococcus aureus*, often encountered on the skin and nasal passages, can manifest within the oral environment, eliciting a spectrum of issues [14]. Notably, it can engender oral abscesses, localized enclaves of inflammation, and pus accumulation, inflicting intense pain and swelling. Moreover, its acidogenic metabolism of dietary sugars can contribute to tooth decay, impelling enamel demineralization and cavity formation [15, 16]. *S. mutans* occupies a central role in dental caries, fueled by its capacity to generate acids upon metabolizing sugars and starches, ultimately eroding tooth enamel [17]. Its pathogenic effects encompass the genesis of cavities via enamel demineralization and its substantial presence in dental plaque, a biofilm that incubates bacterial growth and acid production [18]. *E. faecalis*, typically harbored in the gastrointestinal tract, can extend its presence to the oral milieu. Within dentistry, it poses challenges through its persistence in root canal infections, defying conventional disinfection approaches and leading to protracted treatment and infections. Additionally, it contributes to apical periodontitis, an inflammatory condition at a tooth's root tip. *C. albicans*, an indigenous yeast of the oral cavity, can burgeon under specific circumstances, resulting in infections. Overgrowth can give rise to oral thrush, characterized by whitish patches on the tongue and oral tissues, evoking discomfort, altered taste, and a burning sensation. Moreover, the colonization of denture surfaces can lead to denture stomatitis, sparking inflammation in contact areas [19, 20]. Addressing these dental pathogens, particularly in natural ways, holds significant changes. In this innovative study, we harness the combined potential of CR and zinc oxide nanoparticles (ZnO NPs) to pioneer a targeted and effective approach for combating dental pathogens, including *Staphylococcus aureus*, *Streptococcus mutans*, *Enterococcus faecalis*, and *Candida albicans*. ZnO NPs and CR have been recognized for their significant anticancer properties, and by coupling them both, we aim to enhance their efficacy and deliver a precise drug

treatment strategy. This research endeavors to contribute to the development of advanced interventions in oral health, addressing a pressing need for novel and efficient methods to counteract these challenging microbial adversaries and oral cancer.

## Materials and methods

### Materials

In our previous study, *Kappaphycus alvarezii* samples were collected from Tuticorin, situated along the Southeast coast of the Bay of Bengal, India [21]. Previous research encompassed the fractionation and characterization of CR, where its identity was confirmed through the presence of linear sulfated galactans. These galactans comprise repeating units of D-galactopyranose and 3,6-anhydro- $\alpha$ -D-galactopyranose, linked by  $\alpha(1 \rightarrow 3)$  and  $\beta(1 \rightarrow 4)$ -glycosidic linkages [22]. Additionally, dental pathogens strains encompassing *S. aureus* (MTCC 1144), *S. mutans* (MTCC 497), *E. faecalis* (MTCC 2729), and *C. albicans* (MTCC 183) were sourced from the Department of Microbiology at Saveetha Dental College and Hospitals, Tamil Nadu, India. The essential reagents and materials utilized in this study were obtained from reputable sources: Dulbecco's Modified Eagle's Medium (DMEM), fetal bovine serum (FBS), antibiotic solution, and trypsin were procured from Merck KGaA (Darmstadt, Germany), while 3-(4,5-dimethylthiazol-2-yl)-2,5-diphenyltetrazolium bromide (MTT), 2,2-diphenyl-1-picrylhydrazyl (DPPH), 2,2'-azino-bis(3-ethylbenzothiazoline-6-sulfonic acid) (ABTS), and zinc acetate dihydrate was acquired from Sigma-Aldrich (Mumbai, India). The oral squamous carcinoma (KB) cell lines were purchased from National Centre for Cell Sciences, Pune.

### Preparation of ZnO-CR NPs

A solution of zinc acetate dihydrate (0.1 M) was prepared by dissolving in a mixture of 80 mL ethanol and 20 mL deionized water. Meanwhile, CR was dissolved by adding 0.04 g of CR into 50 mL of deionized water. The CR solution was subjected to heat and stirring to ensure complete dissolution. The dissolved CR solution was then gradually introduced into the zinc acetate solution under continuous stirring for a duration of 30 min, ensuring uniform mixing of the precursors. During this process, the pH of the mixture was carefully monitored and adjusted by the incremental addition of a 1 M NaOH solution. The prepared mixture was further subjected to stirring at a controlled temperature of 60 °C for a period of 3 h. After this step, ultrasonication was employed to enhance dispersion and disrupt any NPs agglomerates. Subsequently, the NPs

dispersion was subjected to centrifugation at 6000 rpm for 15 min to effectively separate any residual larger particles or aggregates from the NP suspension. The obtained NPs dispersion was then dried at 80 °C for 2 h. Characterization of the prepared ZnO-CR NPs was conducted using a comprehensive suite of analytical techniques. X-ray diffraction (XRD) was utilized to assess crystallinity, scanning electron microscopy (SEM) was employed to analyze size and morphology, and Fourier-transform infrared spectroscopy (FTIR) was utilized to examine surface functional groups [23–25].

### Antioxidant assay

#### DPPH assay

The DPPH assay, a widely used method for evaluating antioxidant activity, is based on the principle that DPPH, a stable free radical, undergoes color change from purple to yellow upon receiving an electron from antioxidants. In this study, various concentrations (5, 25, 50, and 100  $\mu\text{g}/\text{mL}$ ) of ZnO-CR NPs were mixed with a 0.1 mM DPPH solution, and the reduction in its absorbance at 517 nm was measured after incubating the mixture for 30 min at room temperature. The extent of color change directly reflects the scavenging potential of the compounds against DPPH radicals. The percentage of DPPH scavenging activity was calculated using  $[(A_{\text{control}} - A_{\text{sample}}) / A_{\text{control}}] \times 100$ , where  $A_{\text{control}}$  is the absorbance of the DPPH solution without the sample, and  $A_{\text{sample}}$  is the absorbance of the sample-DPPH mixture [26].

#### ABTS assay

The ABTS assay, a widely used method for assessing antioxidant activity, operates on the principle that the ABTS radical cation is formed by the oxidation of ABTS with potassium persulfate. The resulting blue-green ABTS radical cation exhibits strong absorbance at 734 nm. In this study, various concentrations (5, 25, 50, and 100  $\mu\text{g}/\text{mL}$ ) of ZnO-CR NPs were added to a prepared ABTS radical cation solution, and the decrease in absorbance was monitored over a 30 min incubation period at room temperature. The extent of absorbance reduction directly correlates with the scavenging potential of the compounds against ABTS radicals. The percentage of ABTS scavenging activity was calculated using  $[(A_{\text{control}} - A_{\text{sample}}) / A_{\text{control}}] \times 100$ , where  $A_{\text{control}}$  is the initial absorbance of the ABTS solution without the sample, and  $A_{\text{sample}}$  is the absorbance of the sample-ABTS mixture after incubation [27].

## Minimal inhibitory concentration (MIC)

The MIC assay for synthesized NPs, a crucial technique in assessing their antimicrobial potential, operates on the principle of determining the lowest concentration of NPs required to inhibit the visible growth of microbial cultures. In this study, synthesized NPs were added at varying concentrations (ranging from 5, 25, 50, and 100  $\mu\text{g}/\text{mL}$ ) to microbial cultures and incubated for 24 h at 37 °C. Following incubation, microbial growth was assessed spectrophotometrically at 600 nm. The MIC was defined as the lowest NP concentration at which no visible growth was observed, indicating an inhibitory effect. Positive (Amoxicillin 50  $\mu\text{g}/\text{mL}$ ) and negative controls (untreated) were included for comparison [28].

## Zone of inhibition

The Zone of Inhibition well diffusion assay, a fundamental technique for evaluating the antimicrobial potential of synthesized NPs, is based on the principle of observing the clear zone formed around the NPs-containing well due to inhibition of microbial growth. In this study, varying concentrations (5, 25, 50, and 100  $\mu\text{g}/\text{mL}$ ) of synthesized NPs were loaded into wells punched into agar plates uniformly inoculated with a standardized microbial culture. The plates were then incubated at 37 °C for 24 h, allowing the NPs to diffuse into the agar. Following incubation, the diameters of the clear zones formed around the wells were measured, reflecting the extent of antimicrobial activity. Larger zone sizes indicated stronger inhibition. Positive (Amoxicillin 50  $\mu\text{g}/\text{mL}$ ) and negative control (untreated) were included for comparative analysis [29].

## Insilico analysis

The molecular docking study aimed to assess the binding energy between the extracted melanin and specific target proteins. The 3D structure of the CR ligand molecule, obtained in SDF format from PubChem (<https://pubchem.ncbi.nlm.nih.gov/>), served as the basis for this analysis. Additionally, the receptor structures of dental pathogens (PDB files 4WVE with a resolution of 1.60 Å, 3BJV with 2.40 Å, 6ORI with 1.40 Å, and 1IYL with 3.20 Å) were acquired from the RCSB Protein Data Bank (PDB) (<https://www.rcsb.org/>). Using Pymol software (Version 1.7.4.5), the ligand molecule was converted from SDF to PDB file format. For the selected proteins, water and other molecules were removed, and the 3D file was saved in the PDB file format. Subsequently, AutoDock 1.5.6 was employed for the molecular docking analysis [30, 31]. The targeted protein PDB files were opened in AutoDock, non-protein and water molecules were removed, and the files

were saved in pdbqt file format. Simultaneously, the ligand molecule underwent conversion from a pdb file to a pdbqt file format, residing in the respective folder. Upon completion of the preparation for the target proteins and ligands, a grid box was generated for the receptor protein and ligand. The grid box was meticulously arranged to encompass both the receptor and ligand, with spacing adjusted to 1 Å. The X, Y, and Z dimensions were then recorded in a text file named "conf" in the respective folder. Subsequently, using the Command Prompt, the docking score was determined. This comprehensive process ensures the meticulous preparation of the ligand and receptor structures and the subsequent execution of molecular docking analysis using AutoDock software Ver1.5.6. The best binding pose was visualized in Discovery Studio software, allowing for the visualization of ligand-receptor interactions, hydrogen bonds, and hydrophobic contacts, offering insights into the binding mechanism. This integrated approach provided valuable information on ligand-receptor interactions and potential binding modes, aiding in the rational design of novel therapeutic compounds [32, 33].

## Antiapoptotic assay

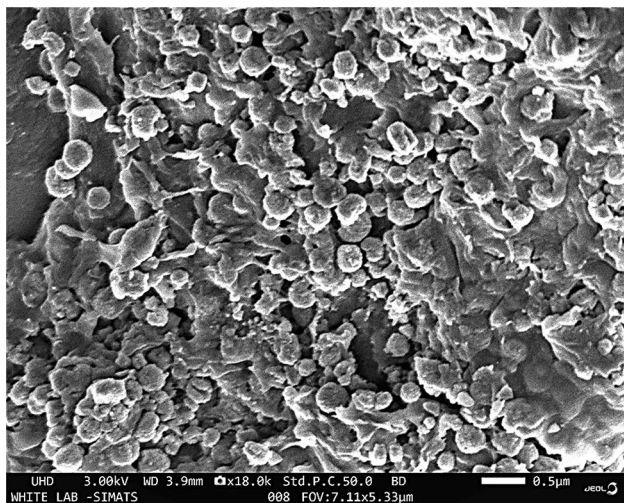
KB cells were seeded at a density of  $5 \times 10^4$ /well in a 96-well plate and allowed to adhere for 24 h. Various concentrations (5, 25, 50, and, 100  $\mu\text{g}/\text{mL}$ ) of ZnO-CR NPs were then added, and the cells were incubated for 48 h. Untreated cells and Triton X-100 were used as control and positive control. Subsequently, MTT reagent (0.5 mg/mL) was added to each well, and the cells were incubated for an additional 4 h. The formazan crystals were dissolved using dimethyl sulfoxide, and the absorbance was measured at 570 nm. The absorbance values were proportional to the number of viable cells and were used to calculate the percentage of cell viability [34].

## Gene expression analysis

In this research, our main objective was to assess the expression of apoptotic genes, namely B-cell lymphoma 2 (BCL2), Bcl-2-associated X-protein (BAX), and tumor protein P53 (P53), in KB cells treated with ZnO-CA NPs. To achieve this, we utilized the Trizol method to extract RNA from dissected tissues [35]. Following this, we conducted RT-PCR analysis using the KAPA SYBR Quick qPCR master mix kit, focusing on specific apoptotic markers outlined in Table 1. We used the GAPDH gene as an internal control for standardization. The relative alterations in gene expression were determined using the  $2^{-\Delta\Delta\text{Ct}}$  method [36].

**Table 1** Primers used for gene expression

Gene	Forward primer (5'–3')	Reverse primer (5'–3')	References
GAPDH	GCCAAAAGGGTCATCATCTCTGC	GGTCACGAGTCCTTCCACGATAC	[37]
BCL-2	GACGACTTCTCCCGCCGCTAC	CGGTTTCAGGTAAGTACAGTCATCCAC	[37]
BAX	AGGTCTTTTTCCGAGTGCCAG	GCGTCCCAAAGTAGGAGAGGAG	[37]
P53	ACATGACGGAGGTTGTGAGG	TGTGATGATGGTGAGGATGG	[38]

**Fig. 1** SEM images of ZnO-CR NPs showed the Spherical shapes

## Statistical analysis

All statistical analyses were performed using GraphPad Prism software Ver 6.0 and analyzed using one-way ANOVA followed by Dunnett's test for multiple comparisons against control. The significance level of  $p < 0.05$  was considered statistically significant. Data are presented as mean  $\pm$  standard deviation (SD) from triplicate experiments.

## Results

### Characterization of ZnO-CR NPs

SEM micrographs (Fig. 1) unveiled the structural characteristics and size distribution of the ZnO-CR NPs. Using Image J software the size of the ZnO-CR NPs was measured. These NPs predominantly displayed a shape reminiscent of spheres. The average particle size was calculated to fall within the range of roughly 100 to 200 nm. The SEM examination indicated that most of the ZnO-CR NPs were evenly distributed, showing minimal tendencies for clustering. The FTIR spectrum of ZnO-CR NPs exhibits characteristic absorption peaks at wavenumbers of  $580\text{ cm}^{-1}$ ,  $658\text{ cm}^{-1}$ ,  $699\text{ cm}^{-1}$ ,  $743\text{ cm}^{-1}$ ,  $842\text{ cm}^{-1}$ ,  $924\text{ cm}^{-1}$ ,  $1043\text{ cm}^{-1}$ ,  $1156\text{ cm}^{-1}$ ,  $1252\text{ cm}^{-1}$ ,  $1371\text{ cm}^{-1}$ ,  $1641\text{ cm}^{-1}$ ,  $1900\text{ cm}^{-1}$ ,  $1996\text{ cm}^{-1}$ ,

$2112\text{ cm}^{-1}$ ,  $2179\text{ cm}^{-1}$ ,  $2230\text{ cm}^{-1}$ ,  $2362\text{ cm}^{-1}$ ,  $2921\text{ cm}^{-1}$ , and  $3372\text{ cm}^{-1}$ , revealing distinct vibrational modes associated with the NPs composition (Fig. 2). The observed peaks suggest the presence of functional groups and potential interactions between ZnO-CR NPs. The lower wavenumber peaks ( $580\text{--}1252\text{ cm}^{-1}$ ) likely signify specific ZnO vibrations and crystal lattice modes, while the higher wavenumber peaks ( $1371\text{--}3372\text{ cm}^{-1}$ ) correspond to CR molecular vibrations, including sulfate group stretching ( $1250\text{--}1350\text{ cm}^{-1}$ ) and hydroxyl groups ( $3400\text{ cm}^{-1}$ ). Compared to previous studies, the presence of specific functional groups associated with sulfate ester, glycosidic linkage, 3,6-anhydro-D-galactose, and D-galactose-4-sulfate represents the characteristic wavenumbers of CR [39]. The shifts and intensities of these peaks may indicate potential chemical bonding or interactions, implying the formation of a NP structure. Further analysis is essential to elucidate the nature of these interactions and their relevance in the context of potential applications for the NPs system. The XRD analysis of the ZnO-CR NPs reveals a dominant and sharp peak at  $31.764^\circ$ , indicative of a well-defined crystalline phase (Fig. 3). The presence of this prominent peak suggests the predominant crystalline nature of the composite material in this particular crystallographic direction. The relatively uniform intensity of the other peaks implies a consistent distribution of crystallographic orientations within the NPs structure. The calculated crystallinity of 89.4% reflects the proportion of the material's crystalline regions, while the amorphous fraction accounts for 10.6%, signifying areas lacking a regular crystal lattice. This ZnO-CR NPs XRD profile indicates the coexistence of crystalline and amorphous components, potentially resulting from interactions between ZnO and CR.

### Free radical scavenging effect of ZnO-CR NPs

The DPPH assay demonstrates a dose-dependent scavenging effect of ZnO-CR NPs on DPPH free radicals, with scavenging activity increasing as their concentration rises ( $5\text{ }\mu\text{g/mL}$ ,  $25\text{ }\mu\text{g/mL}$ ,  $50\text{ }\mu\text{g/mL}$ , and  $100\text{ }\mu\text{g/mL}$ ), resulting in scavenging percentages of 7%, 22%, 43%, and 64%, respectively (Fig. 4A). To evaluate its antioxidant potential, ZnO-CR NPs are compared to trolox, a widely recognized antioxidant. At corresponding concentrations ( $5\text{ }\mu\text{g/mL}$ ,  $25\text{ }\mu\text{g/mL}$ ,  $50\text{ }\mu\text{g/mL}$ , and  $100\text{ }\mu\text{g/mL}$ ), Trolox exhibits higher DPPH radical scavenging percentages of 14%, 29%, 52%, and 72%.

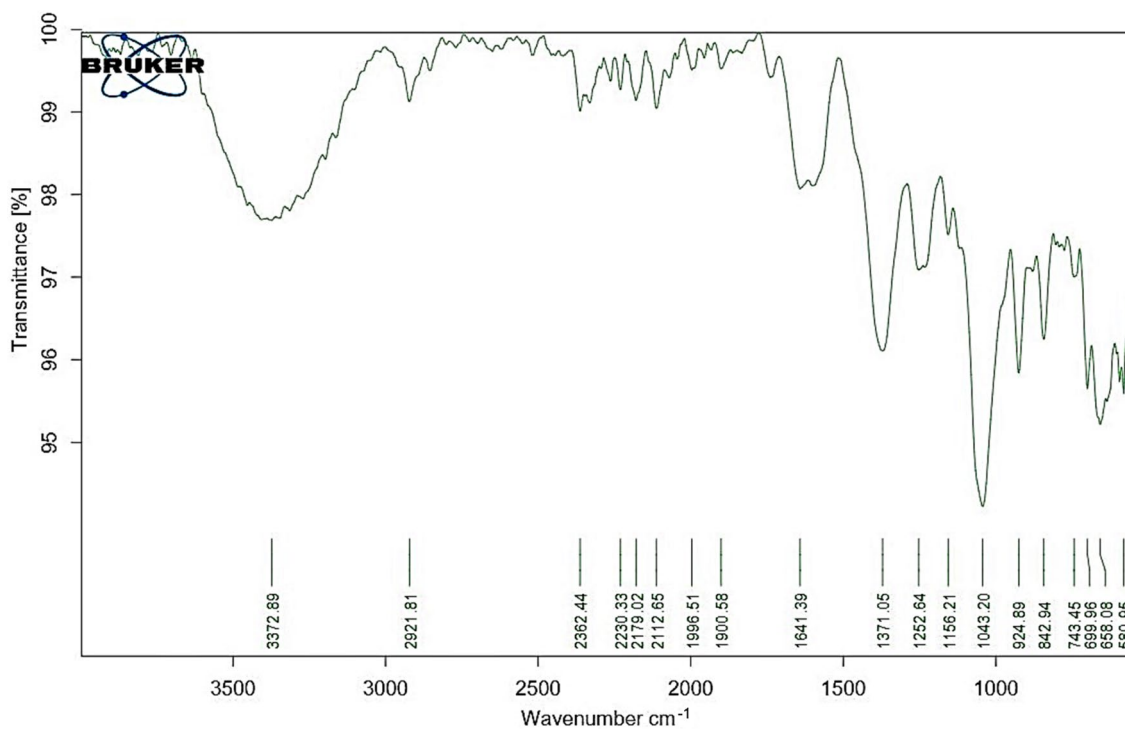


Fig. 2 FTIR characterization of ZnO-CR NPs

COMMANDER Sample ID (Coupled TwoTheta/Theta)

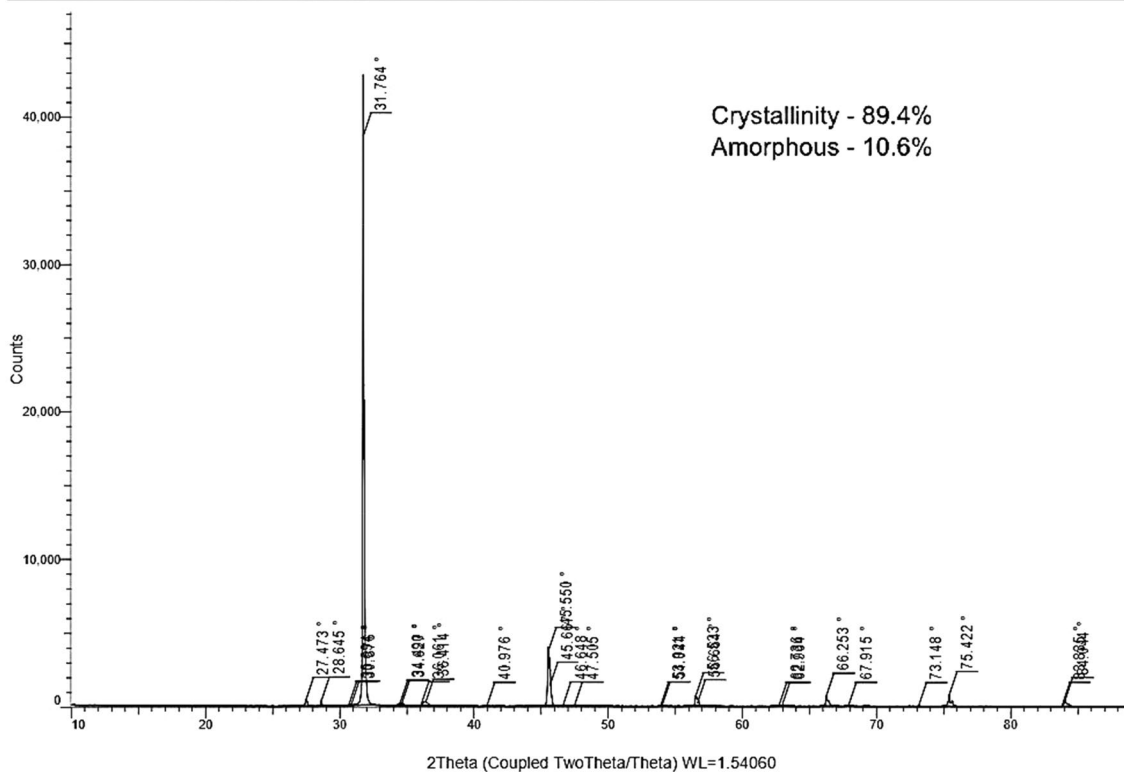
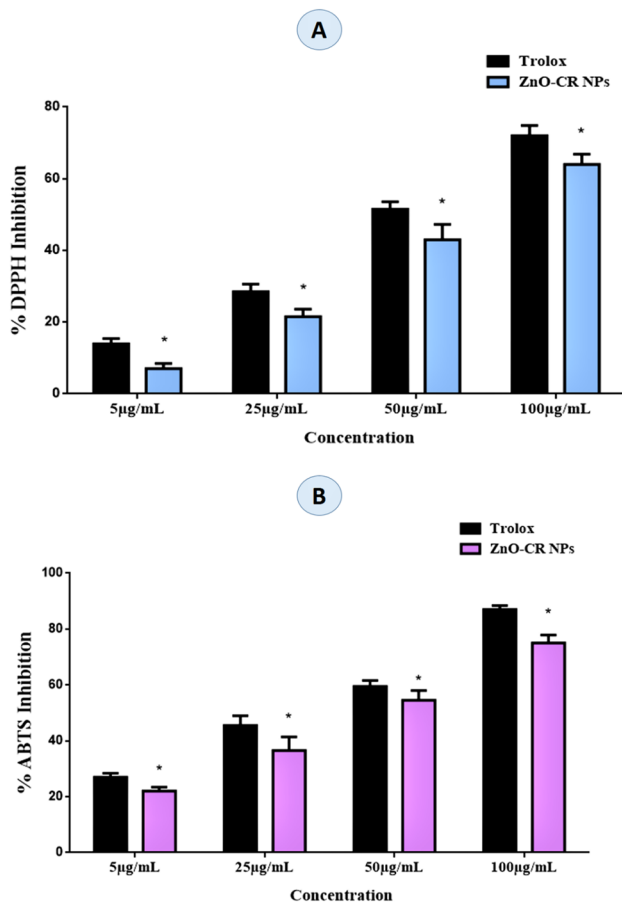
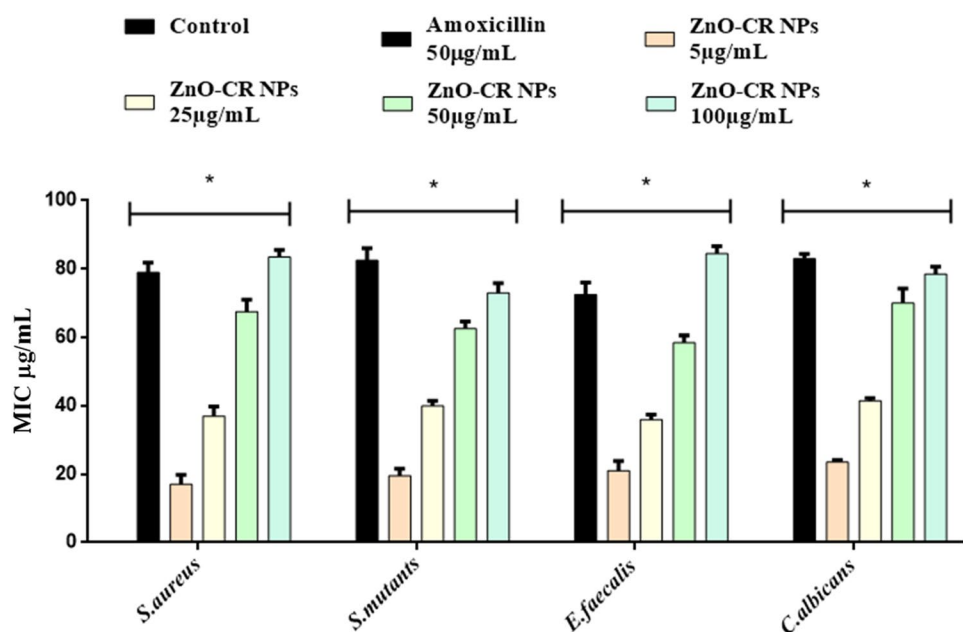


Fig. 3 XRD analysis of ZnO-CR NPs



**Fig. 4** Free radical scavenging activity of ZnO-CR NPs (5 µg/mL, 25 µg/mL, 50 µg/mL, and 100 µg/mL) on **A** DPPH and **B** ABTS. Trolox was used as a positive control. The \* represented the level of significance ( $p < 0.05$ ) when the results were compared to the control. Data were presented as mean  $\pm$  SD of three independent experiments

**Fig. 5** MIC of ZnO-CR NPs at different concentration against dental pathogens of *S. aureus*, *S. mutans*, *E. faecalis*, and *C. albicans*. Amoxicillin was used as a positive control. The \* represented the level of significance ( $p < 0.05$ ) when the results were compared to the control. Data were presented as mean  $\pm$  SD of three independent experiments



Remarkably, ZnO-CR NPs demonstrate a significant capacity to neutralize DPPH radicals, with scavenging percentages closely resembling those of trolox across all concentrations. Notably, at 25 µg/mL and 50 µg/mL concentrations, ZnO-CR NPs exhibit scavenging activity equivalent to trolox.

The ABTS assay reveals a dose-dependent scavenging effect of ZnO-CR NPs on ABTS free radicals. As the concentration of ZnO-CR NPs increases (5 µg/mL, 25 µg/mL, 50 µg/mL, and 100 µg/mL), the percentage of ABTS radical scavenging activity progressively rises, resulting in scavenging percentages of 22%, 37%, 55%, and 75%, respectively (Fig. 4B). In comparison, the antioxidant capacity of ZnO-CR NPs is assessed against trolox, a well-established antioxidant. At equivalent concentrations (5 µg/mL, 25 µg/mL, 50 µg/mL, and 100 µg/mL), Trolox demonstrates higher ABTS radical scavenging percentages of 27%, 46%, 60%, and 87%. Notably, ZnO-CR NPs display a substantial capacity to neutralize ABTS radicals, and their scavenging activity closely mirrors that of Trolox across all concentrations. These findings highlight the potential of ZnO-CR NPs as a potent natural antioxidant.

#### Antimicrobial activity of ZnO-CR NPs

The experiment involving various concentrations (5 µg/mL, 25 µg/mL, 50 µg/mL, and 100 µg/mL) of ZnO-CR NPs against dental pathogens yielded consistent MIC values (Fig. 5). ZnO-CR NPs demonstrated comparable MIC values across the tested dental pathogens, indicating a uniform inhibitory effect. Notably, *S. aureus*, *S. mutans*, *E. faecalis*, and *C. albicans* exhibited increased susceptibility to ZnO-CR NPs, characterized by lower MIC values of 50 µg/mL. This signifies that concentrations equal to or exceeding

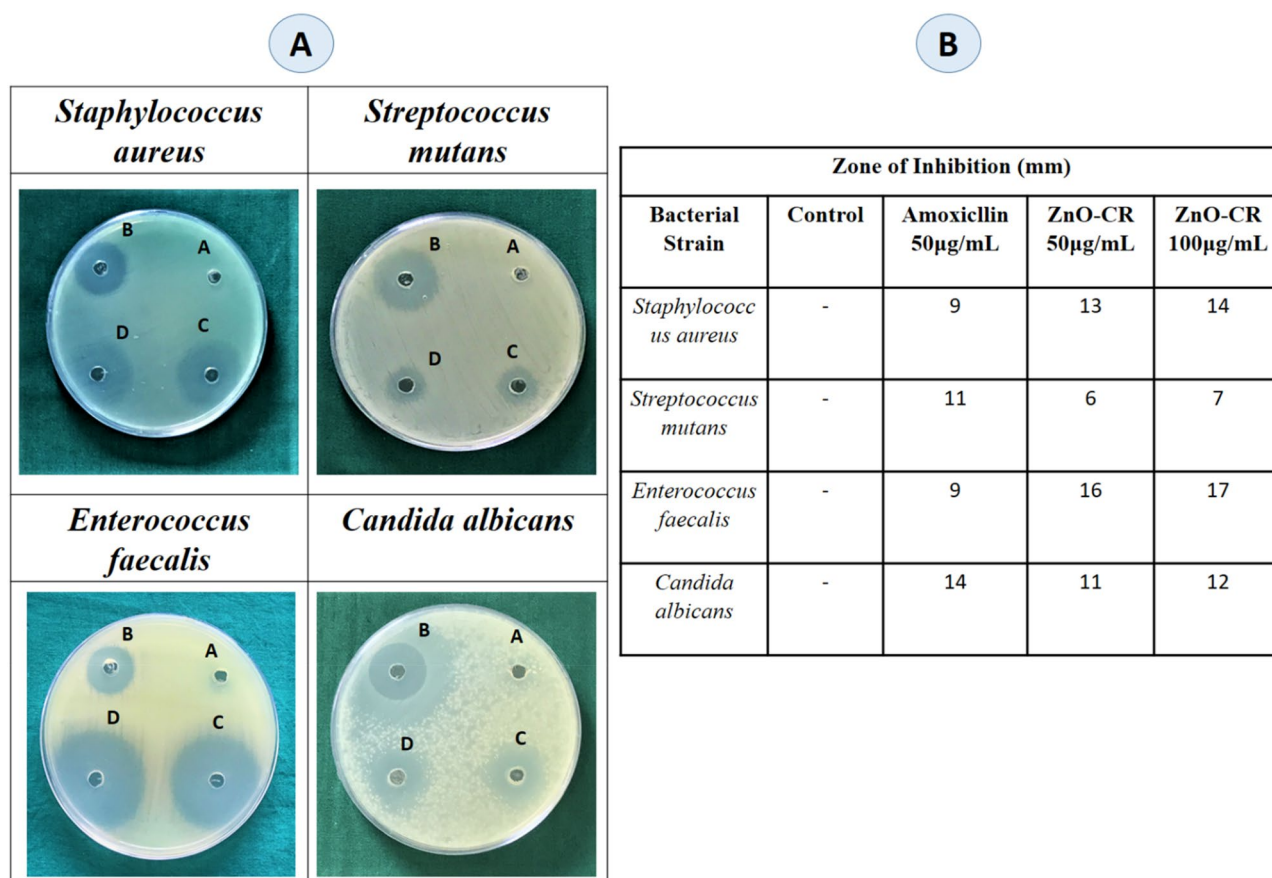
50  $\mu\text{g}/\text{mL}$  of ZnO-CR NPs effectively hindered the growth of these dental pathogens. In that case, ZnO-CR NPs have demonstrated a potential to act as a potent antimicrobial agent against a range of dental pathogens, with the ability to suppress their growth at clinically relevant concentrations. This finding suggests the promising utility of ZnO-CR NPs in combating oral infections and promoting oral health.

The zone of inhibition assay results demonstrated the antimicrobial efficacy of ZnO-CR NPs against all tested dental pathogens. At a concentration of 50  $\mu\text{g}/\text{mL}$ , ZnO-CR NPs displayed zones of inhibition ranging from 13 mm, 6 mm, 16 mm, to 11 mm for *S. aureus*, *S. mutans*, *E. faecalis*, and *C. albicans*, respectively. When the concentration was increased to 100  $\mu\text{g}/\text{mL}$ , the zones of inhibition expanded to 14 mm, 7 mm, 17 mm, and 12 mm, respectively, indicating a more pronounced inhibitory effect. Comparatively, the positive control, amoxicillin (50  $\mu\text{g}/\text{mL}$ ), exhibited zones of inhibition measuring 9 mm, 11 mm, 9 mm, and 14 mm for the respective dental pathogens (Fig. 6). These results underscore the potent antimicrobial activity of ZnO-CR NPs, as they successfully inhibited the growth of all tested dental pathogens, with an efficacy comparable to that of the

established antimicrobial agent amoxicillin. The increasing zones of inhibition with higher ZnO-CR NP concentrations further emphasize their potential as a valuable antimicrobial agent for addressing oral infections caused by these pathogens.

### Interaction between CR and dental pathogen receptor

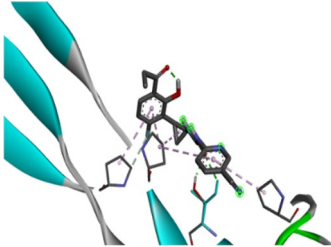
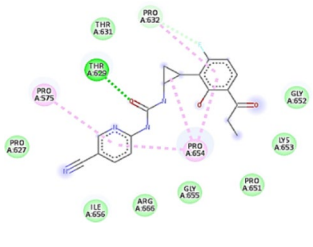
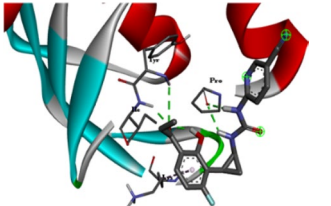
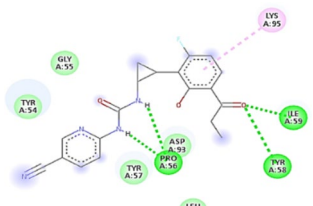
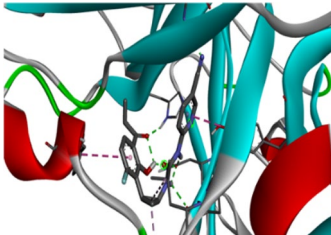
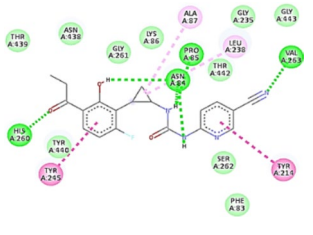
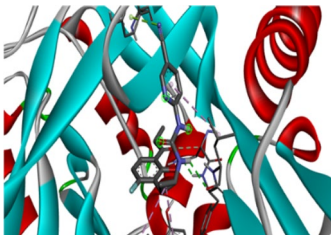
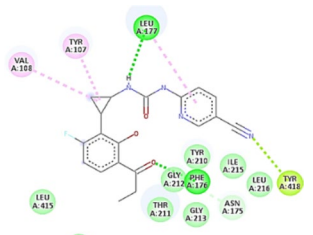
The results of the molecular docking analysis provide valuable insights into the potential interactions between CR and the receptor proteins of four distinct dental pathogens, namely *S. aureus*, *S. mutans*, *E. faecalis*, and *C. albicans* (Table 2). In the first docking study involving *S. aureus*, the interaction with the surface protein G (PDB ID: 4WVE) yielded a remarkable binding affinity value of  $-8.46$  kcal/mol. This strongly negative value indicates a robust and energetically favorable interaction between CR and the *S. aureus* receptor. The docking simulation pinpointed specific amino acids that participated in this interaction, including PRO, PRO, THR, THR, and PRO. For the *S. mutans* docking study with PTSIIA (PDB ID: 3BJV), the calculated binding



**Fig. 6** Zone of inhibition of different dental pathogens by ZnO-CR NPs. **A** A—Control, B—Amoxicillin (50  $\mu\text{g}/\text{mL}$ ), C—ZnO-CR NPs at 25  $\mu\text{g}/\text{mL}$ , and D—ZnO-CR NPs at 50  $\mu\text{g}/\text{mL}$ . **B** Zone of inhibition measured at mm



**Table 2** 3D and 2D representative images of  $\kappa$ -carrageenan with dental pathogen receptor interactions. 4WVE (*Staphylococcus aureus* surface protein G), 3BJV (PTSIIA), 6ORI (Enterococcal surface protein), and 1IYL (N-myristoyl transferase)

Protein	Ligand	Binding affinity (kcal/mol)	Amino acid interaction	
			3D interactions	2D interactions
4WVE	$\kappa$ -carrageenan	-8.46		
3BJV	$\kappa$ -carrageenan	-5.14		
6ORI	$\kappa$ -carrageenan	-8.88		
1IYL	$\kappa$ -carrageenan	-7.56		

affinity was -5.14 kcal/mol. While slightly less negative than the previous case, this value still indicates a favorable interaction between CR and the *S. mutans* receptor. The docking analysis highlighted interactions with LYS, PRO, ASP, ILE, and TYR. In the context of *E. faecalis*, the docking study with Enterococcal surface protein (PDB ID: 6ORI) exhibited a high binding affinity value of -8.88 kcal/mol. This suggests a strong and energetically favorable interaction between CR and the *E. faecalis* receptor. The docking analysis identified interactions with HIS, TYR, ASN, ALA, LEU, VAL, and TYR. Lastly, the docking analysis involving *C. albicans* N-myristoyltransferase (PDB ID: 1IYL) and CR resulted in a binding affinity value of -7.56 kcal/mol. While slightly less negative than some previous cases, this value still indicates a favorable interaction. The docking study revealed interactions with LEU, VAL, TYR, PHE, and TYR.

These results suggest that these amino acids contribute to the formation of stable interactions between CR and the dental pathogen receptor through potential hydrogen bonding, electrostatic interactions, or hydrophobic contacts.

### Anticancer activity of ZnO-CR NPs

The MTT assay evaluates cell viability by measuring the conversion of a yellow tetrazolium salt into a purple formazan product by living cells. The results of the MTT assay (Fig. 7) indicate notable variations in the morphology and viability of KB cells as the concentrations of ZnO-CR NPs increase. At lower concentrations (5  $\mu$ g/mL), there was minimal impact on cell viability after 24 h of exposure. In contrast, the Cyclophosphamide group exhibited a significant reduction in cell viability (29%).

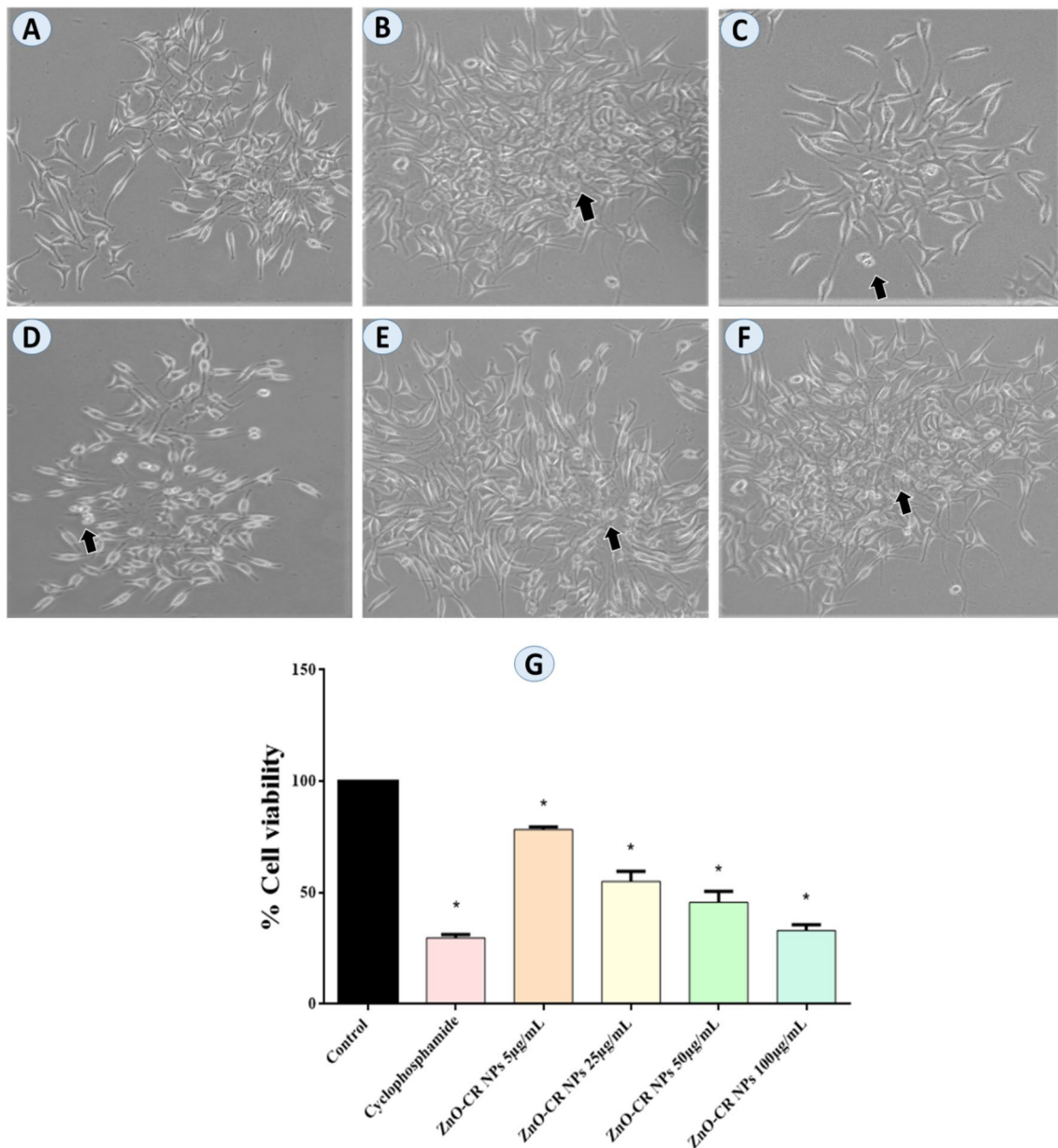


**Fig. 7** In-vitro anticancer activity of ZnO-CR NPs tested on KB cells by MTT assay. The different groups are Untreated control cells (A), Cyclophosphamide group (50 µg/mL) (positive control) (B), ZnO-CR NPs (5 µg/mL, 25 µg/mL, 50 µg/mL, and 100 µg/mL) (C, D, E and F). G Graph showing the percentage of cell viability on A375 can-

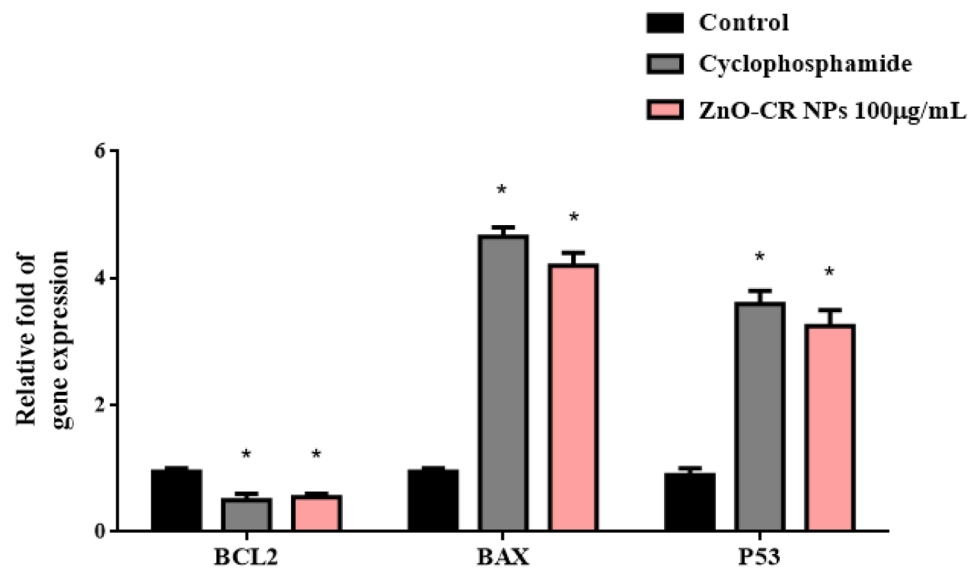
cer cells at different concentrations of melanin. The black arrow indicates the morphological changes in the cells due to apoptosis. The \* represented the level of significance ( $p < 0.05$ ) when the results were compared to the control. Data were presented as mean  $\pm$  SD of three independent experiments

Meanwhile, at higher concentrations (100 µg/mL), a substantial decrease in KB cell viability (33%) was observed, resembling the cell viability in the positive control group. These findings suggest that ZnO-CR NPs exhibit cytotoxic effects on KB cells at the tested concentrations. The significant alterations in KB cell viability associated with the escalating concentrations of ZnO-CR NPs imply their potential utility in dental applications.

### Apoptotic gene expression level

Among the various concentrations tested, the highest concentration of ZnO-CR NPs at 100 µg/mL exhibited superior antioxidant, antimicrobial, and antiapoptotic activity compared to the other groups. Therefore, this 100 µg/mL concentration was chosen as the optimal dosage for further investigation in gene expression studies. Previous research

**Fig. 8** Effect of ZnO-CR NPs treatment group on the mRNA expression level of BCL2, BAX, and P53. Data were expressed as mean + SD of three independent experiments. \* $p < 0.05$  as compared to the control



has indicated that to exhibit anticancer activity, a substance should reduce BCL2 expression while increasing the levels of BAX and P53 [37]. Consistent with these findings, our study demonstrated that KB cells treated with ZnO-CR NPs at 100 µg/mL showed a significant decrease ( $p < 0.05$ ) in BCL2 expression (0.6 fold) and an upregulation of BAX (4.2 fold) and P53 (3.3 fold) levels when compared to the control group (Fig. 8). These collective findings suggest that ZnO-CR NPs have the potential to enhance the apoptotic mechanism, leading to cell death in cancer cells.

## Discussion

Combining compounds with NPs can lead to synergistic effects, where the combined treatment is more potent than either compound alone. The NPs can enhance the activity of the compounds and promote their interaction with pathogens, resulting in a stronger antimicrobial and anticancer effect [40]. ZnO NPs exhibit strong antimicrobial activity against a wide range of microorganisms, including bacteria, fungi, and viruses [41]. In dentistry, they can help prevent and control oral infections, such as dental caries, gingivitis, and periodontitis [42, 43]. ZnO NPs can combat drug resistance that some oral pathogens develop against traditional antibiotics. Their multiple mechanisms of action, such as disrupting cell membranes and generating reactive oxygen species (ROS), make it more difficult for bacteria to develop resistance [44]. In this study, the ZnO-CR NPs were synthesized to analyze their effective antimicrobial activity against different pathogens such as *S. aureus*, *S. mutans*, *E. faecalis*, and *C. albicans*. Further, their role in anticancer activity was investigated in the KB cells.

The amalgamation of structural insights gleaned from SEM, compositional information obtained through FTIR, and crystalline revelation from XRD characterization collectively shed light on the potential antimicrobial activity of the synthesized ZnO-CR NPs. Similar to previous studies, these NPs exhibited a spherical shape [45]. The SEM results, portraying NPs with a spherical morphology and uniform size distribution, are advantageous for their potential antimicrobial efficacy. The nanoscale dimensions and even distribution could facilitate efficient interaction with microbial cells, providing a larger surface area for contact and disruption. A recent study states that the minimal clustering observed in SEM images implies that the NPs could be effectively dispersed in antimicrobial applications, enhancing their coverage and effectiveness against pathogens [46, 47]. The FTIR analysis, revealing absorption peaks indicative of distinct vibrational modes associated with ZnO and CR, accentuates the possibility of multifaceted antimicrobial mechanisms. The observed absorption peaks corresponding to specific molecular vibrations in CR, such as sulfate group stretching and hydroxyl groups, suggest the involvement of these groups in interactions with microbial surfaces. These interactions could potentially disrupt bacterial membranes and hinder their growth, contributing to the antimicrobial effect [48, 49]. The XRD analysis indicates the well-defined crystalline nature of the NPs, which aligns with ZnO's well-documented antimicrobial properties. The dominant and sharp peak at  $31.764^\circ$  signifies the presence of a crystalline phase, crucial for ZnO's ability to generate ROS upon exposure to external stimuli. These ROS can inflict damage on microbial cell membranes, nucleic acids, and proteins, thereby inhibiting bacterial growth and rendering them less virulent. The coexistence of crystalline and amorphous components, as indicated by the calculated crystallinity and amorphous

fraction, could be advantageous for their antimicrobial activity [50]. This structural feature might enhance the overall surface reactivity, providing a platform for both the direct antimicrobial effects of ZnO and the potential interactions facilitated by CR's molecular groups. Considering the cumulative evidence from SEM, FTIR, and XRD analyses, the synthesized ZnO-CR NPs present a promising outlook for antimicrobial applications.

Some dental pathogens, like *S. mutans*, generate ROS as a defense mechanism or as part of their virulence strategy. These ROS can damage host tissues and contribute to the progression of oral diseases. They can form biofilms on dental surfaces, which are complex communities of microorganisms embedded in a matrix [51]. ROS generated by pathogens in biofilms can contribute to their stability and resistance to treatment. Antioxidants can counteract the harmful effects of pathogenic ROS, disrupt biofilm formation, weaken the protective matrix, and make it easier to eliminate pathogens [52]. The antioxidant assay reveals that ZnO-CR NPs effectively scavenge DPPH and ABTS free radicals, and this scavenging activity increases with higher concentrations. This dose-dependent behavior suggests that as the concentration of ZnO-CR NPs increases, more NPs are available to neutralize the free radicals. The substantial scavenging percentages, although slightly lower than those of Trolox, imply that ZnO-CR NPs have a notable ability to donate electrons to neutralize DPPH and ABTS radicals. This process is indicative of a hydrogen atom transfer mechanism, where the NPs' constituents, ZnO and CR, likely contribute to the overall antioxidant activity. This result correlates with previous research indicating that CR hydrogel with ZnO NPs effectively showed antioxidant activity [53]. The mechanisms underlying the antioxidant activity of ZnO-CR NPs are likely multifaceted. ZnO, as a well-studied antioxidant material, can generate ROS such as superoxide radicals and hydroxyl radicals upon interaction with water and oxygen. These ROS can then react with and neutralize free radicals, effectively breaking the chain of radical propagation. Additionally, the CR component might contribute to the antioxidant activity through its molecular groups, such as hydroxyl groups and sulfate groups. These groups can act as hydrogen donors, participating in radical-scavenging reactions. The interaction between ZnO and CR could potentially enhance the overall antioxidant efficacy of the NPs. ZnO's ROS-generating ability could synergize with CR's hydrogen-donating groups, resulting in a combined antioxidant effect. The close resemblance of scavenging percentages to Trolox suggests that the ZnO-CR NPs exhibit comparable antioxidant potential to a well-established antioxidant compound. Meanwhile, the observed non-toxicity aligns with the ZnO-CR NPs potential antimicrobial and antioxidant properties, making them an attractive candidate for dental materials or formulations. The stable and

unaffected viability of DPSCs in the presence of ZnO-CR NPs across the concentration range of 5 to 100  $\mu\text{g}/\text{mL}$  indicates a high degree of biocompatibility. This observation is crucial for potential biomedical applications, as the absence of cytotoxic effects is a key requirement for any material intended for use within the human body. Incorporating ZnO-CR NPs into dental materials, such as coatings, toothpaste, or mouthwash, could potentially harness their antimicrobial effects to prevent oral infections and maintain oral hygiene. Moreover, their antioxidant properties could contribute to combating oxidative stress-related issues often associated with oral health.

The consistent MIC values observed across various dental pathogens when exposed to different concentrations of ZnO-CR NPs highlight their potential as effective antimicrobial agents in dental applications. The notable susceptibility of important dental pathogens such as *S. aureus*, *S. mutans*, *E. faecalis*, and *C. albicans* to ZnO-CR NPs at a concentration of 50  $\mu\text{g}/\text{mL}$  demonstrates their potent antimicrobial activity. These findings are by the previous research suggesting that the efficacy can be attributed to the NP's capability to disrupt cell membranes, interfere with essential cellular processes, and generate ROS, collectively leading to the inhibition of the growth of these pathogens [53]. The observed expansion of inhibitory zones in a dose-dependent manner within the zone of inhibition assay further emphasizes the inhibitory effect of these NPs. This characteristic holds significant promise for the development of localized treatments. Further, the outcomes of the molecular docking analysis shed light on the potential mechanisms underlying the antimicrobial activity of CR against various dental pathogens, including *S. aureus*, *S. mutans*, *E. faecalis*, and *C. albicans*. The strong negative binding affinity values obtained in the docking studies indicate favorable interactions between CR and the respective receptor proteins of these pathogens. In the case of *S. aureus*, the binding affinity between CR and the surface protein G suggests that CR could potentially disrupt the interaction of this protein with its native ligands, affecting the pathogen's ability to adhere to host cells or surfaces. Similarly, the interactions between CR and PTSIIA in *S. mutans* could impede sugar transport, which is vital for the growth of this bacterium [54]. The binding affinity of CR with Enterococcal surface protein in *E. faecalis* hints at a potential interference with cellular adhesion, colonization, or virulence mechanisms, ultimately hindering the pathogen's ability to cause infection [55]. For *C. albicans*, the interaction with N-myristoyltransferase implies a potential disruption of protein myristoylation, which is essential for its cellular processes [56]. These docking results suggest that CR could interfere with critical molecular processes involved in pathogen adhesion, colonization, and growth. By binding to specific receptor proteins, CR may prevent these pathogens from attaching to host tissues, thwarting their ability to

establish infections. From this antimicrobial analysis, incorporating ZnO-CR NPs into dental materials or treatments could mitigate the growth of pathogenic microorganisms, hinder biofilm formation, and promote oral health. While further research is necessary to understand their mechanisms fully, interactions with oral tissues, and long-term safety, the consistent and potent antimicrobial activity of ZnO-CR NPs suggests their potential as innovative tools for addressing oral infections and preventing antimicrobial resistance.

Oral cancers, which include types like squamous cell carcinoma (such as KB Cells), often originate as localized lesions or precancerous growths [57]. NPs possessing anticancer properties can be tailored to selectively target these early-stage or precancerous cells, thereby preventing their progression into full-fledged cancer. Such NPs, capable of targeting and impeding the growth of cancer cells within the oral cavity, hold promise for early intervention. Detecting and addressing oral cancer in its early stages significantly enhances the likelihood of successful treatment and reduces the need for aggressive and debilitating therapies [58]. Recent studies have shown that CR exhibited the ability to inhibit tumor growth and it enhanced adjuvant activity by stimulating the immune response in cancer immunotherapy [59]. In our study, ZnO-CR NPs demonstrated a substantial reduction in KB cell viability, and we investigated their mechanism of anticancer action through the expression of apoptotic genes. The modulation of apoptotic genes, specifically BCL2, BAX, and P53, is a pivotal aspect of anticancer activity. Apoptosis, also known as programmed cell death, is a highly regulated cellular process essential for maintaining tissue equilibrium and preventing the development and progression of cancers [60]. BCL2 is an anti-apoptotic gene responsible for encoding a protein that inhibits apoptosis by preventing the release of cytochrome c from the mitochondria, a critical step in the apoptotic pathway. Conversely, BAX is a pro-apoptotic gene that encodes a protein promoting apoptosis by permeabilizing the mitochondrial outer membrane, enabling the release of apoptotic factors into the cytoplasm. P53 is a well-established tumor suppressor gene that plays a central role in cancer prevention by regulating cell cycle arrest, DNA repair, and apoptosis in response to DNA damage or cellular stress [61]. Taken together, our results indicate that ZnO-CR NPs target the apoptotic pathway involving BCL2, BAX, and P53 to inhibit the growth of KB cancerous cells.

## Conclusion

In conclusion, the combination of ZnO-CR NPs demonstrates potent antimicrobial and anticancer properties. Their antiapoptotic property make them a promising drug for dental oral cancer applications. ZnO-CR NPs effectively inhibit

various dental pathogens, offering localized treatments. Molecular docking suggests potential interference with pathogen adhesion. The consistent and potent anticancer and antimicrobial effects demonstrated by these NPs offer a promising strategy to effectively address oral cancer and combat the growing challenge of antimicrobial resistance.

**Acknowledgements** The authors acknowledge Dr. Mukesh Doble, Department of Cariology, Saveetha Dental College and Hospitals, SIMATS, Chennai 600 077, Tamil Nadu, India for providing the  $\kappa$ -carrageenan to carry out this study. The authors acknowledge the funding from Researchers Supporting Project number (RSPD2024R665), King Saud University, Riyadh, Saudi Arabia.

**Author contributions** VM, MSKK, MRS, BS, JG: Conceptualization, methodology, and validation. ZAK, AG: Writing original draft and supervision.

**Funding** The authors acknowledge the funding from Researchers Supporting Project number (RSPD2024R665), King Saud University, Riyadh, Saudi Arabia.

**Data availability** Data will be made available on request.

## Declarations

**Conflict of interest** All the authors declare no conflict of interest regarding this work.

**Ethical approval** Not Applicable.

**Consent to participate** Not applicable.

**Consent to publish** Not applicable.

## References

- Rupert R, Rodrigues KF, Thien VY, Yong WTL (2022) Carrageenan from *kappaphycus alvarezii* (Rhodophyta, Solieriaceae): metabolism, structure, production, and application. *Front Plant Sci.* <https://doi.org/10.3389/fpls.2022.859635>
- Hurtado AQ, Critchley AT (2018) A review of multiple biostimulant and bioeffector benefits of AMPEP, an extract of the brown alga *Ascophyllum nodosum*, as applied to the enhanced cultivation and micropropagation of the commercially important red algal carrageenophyte *Kappaphycus alvarezii*. *J Appl Phycol* 30:2859–2873. <https://doi.org/10.1007/s10811-018-1407-4>
- Hans N, Gupta S, Pattnaik F et al (2023) Valorization of *Kappaphycus alvarezii* through extraction of high-value compounds employing green approaches and assessment of the therapeutic potential of  $\kappa$ -carrageenan. *Int J Biol Macromol* 250:126230. <https://doi.org/10.1016/j.ijbiomac.2023.126230>
- Khotimchenko M, Tiaso V, Kalitnik A et al (2020) Antitumor potential of carrageenans from marine red algae. *Carbohydr Polym* 246:116568. <https://doi.org/10.1016/j.carbpol.2020.116568>
- Liu Z, Gao T, Yang Y et al (2019) Anti-cancer activity of porphyrin and carrageenan from red seaweeds. *Molecules* 24:4286. <https://doi.org/10.3390/molecules24234286>
- Gupta P, Goel A, Singh KR et al (2021) Dissecting the anti-biofilm potency of kappa-carrageenan capped silver nanoparticles

- against *Candida* species. *Int J Biol Macromol* 172:30–40. <https://doi.org/10.1016/j.ijbiomac.2021.01.035>
7. Martiny TR, Pacheco BS, Pereira CMP et al (2020) A novel biodegradable film based on  $\kappa$ -carrageenan activated with olive leaves extract. *Food Sci Nutr* 8:3147–3156. <https://doi.org/10.1002/fsn3.1554>
  8. Nouri A, Tavakkoli Yarak M, Ghorbanpour M, Wang S (2018) Biodegradable  $\kappa$ -carrageenan/nanoclay nanocomposite films containing *Rosmarinus officinalis* L. extract for improved strength and antibacterial performance. *Int J Biol Macromol* 115:227–235. <https://doi.org/10.1016/j.ijbiomac.2018.04.051>
  9. Zepon KM, Martins MM, Marques MS et al (2019) Smart wound dressing based on  $\kappa$ -carrageenan/locust bean gum/cranberry extract for monitoring bacterial infections. *Carbohydr Polym* 206:362–370. <https://doi.org/10.1016/j.carbpol.2018.11.014>
  10. Shukla PS, Borza T, Critchley AT, Prithiviraj B (2016) Carrageenans from red seaweeds as promoters of growth and elicitors of defense response in plants. *Front Mar Sci*. <https://doi.org/10.3389/fmars.2016.00081>
  11. Cunha L, Grenha A (2016) Sulfated seaweed polysaccharides as multifunctional materials in drug delivery applications. *Mar Drugs* 14:42. <https://doi.org/10.3390/md14030042>
  12. Jagtap P, McGowan T, Bandhakavi S et al (2012) Deep metaproteomic analysis of human salivary supernatant. *Proteomics* 12:992–1001. <https://doi.org/10.1002/pmic.201100503>
  13. Llewellyn C, Johnson N, Warnakulasuriya KAA (2001) Risk factors for squamous cell carcinoma of the oral cavity in young people—a comprehensive literature review. *Oral Oncol* 37:401–418. [https://doi.org/10.1016/S1368-8375\(00\)00135-4](https://doi.org/10.1016/S1368-8375(00)00135-4)
  14. Masiuk H, Wcislek A, Jursa-Kulesza J (2021) Determination of nasal carriage and skin colonization, antimicrobial susceptibility and genetic relatedness of *Staphylococcus aureus* isolated from patients with atopic dermatitis in Szczecin. *Poland BMC Infect Dis* 21:701. <https://doi.org/10.1186/s12879-021-06382-3>
  15. Kobayashi SD, Malachowa N, DeLeo FR (2015) Pathogenesis of *Staphylococcus aureus* Abscesses. *Am J Pathol* 185:1518–1527. <https://doi.org/10.1016/j.ajpath.2014.11.030>
  16. Koo H, Andes DR, Krysan DJ (2018) *Candida*–streptococcal interactions in biofilm-associated oral diseases. *PLOS Pathog* 14:e1007342. <https://doi.org/10.1371/journal.ppat.1007342>
  17. Matsui R, Cvitkovich D (2010) Acid tolerance mechanisms utilized by *Streptococcus mutans*. *Future Microbiol* 5:403–417. <https://doi.org/10.2217/fmb.09.129>
  18. Priya A, Kumar CBM, Valliammai A et al (2021) Usnic acid deteriorates acidogenicity, aciduranc and glucose metabolism of *Streptococcus mutans* through downregulation of two-component signal transduction systems. *Sci Rep* 11:1374. <https://doi.org/10.1038/s41598-020-80338-6>
  19. Takakura N, Sato Y, Ishibashi H et al (2003) A novel murine model of oral candidiasis with local symptoms characteristic of oral thrush. *Microbiol Immunol* 47:321–326. <https://doi.org/10.1111/j.1348-0421.2003.tb03403.x>
  20. Pereira-Cenci T, Del Bel Cury AA, Crieleard W, Ten Cate JM (2008) Development of *Candida*-associated denture stomatitis: new insights. *J Appl Oral Sci* 16:86–94. <https://doi.org/10.1590/S1678-77572008000200002>
  21. Raman M, Doble M (2015)  $\kappa$ -Carrageenan from marine red algae, *Kappaphycus alvarezii* - A functional food to prevent colon carcinogenesis. *J Funct Foods* 15:354–364. <https://doi.org/10.1016/j.jff.2015.03.037>
  22. Raman M, Doble M (2014) Physicochemical and structural characterisation of marine algae *Kappaphycus alvarezii* and the ability of its dietary fibres to bind mutagenic amines. *J Appl Phycol* 26:2183–2191. <https://doi.org/10.1007/s10811-014-0241-6>
  23. Alsahli MS, Devanesan S, Atif M et al (2020) Therapeutic potential assessment of green synthesized zinc oxide nanoparticles derived from fennel seeds extract. *Int J Nanomed* 15:8045–8057. <https://doi.org/10.2147/IJN.S272734>
  24. Ondijo C, Kengara F, K’Owino I (2022) Synthesis, characterization, and evaluation of the remediation activity of *Cissus quadrangularis* zinc oxide nanoparticle-activated carbon composite on dieldrin in aqueous solution. *J Nanotechnol* 2022:1–17. <https://doi.org/10.1155/2022/2055024>
  25. Ogunyemi SO, Abdallah Y, Zhang M et al (2019) Green synthesis of zinc oxide nanoparticles using different plant extracts and their antibacterial activity against *Xanthomonas oryzae* pv. *oryzae*. *Artif Cells, Nanomed, Biotechnol* 47:341–352. <https://doi.org/10.1080/21691401.2018.1557671>
  26. Murugan R, Mukesh G, Haridevamuthu B et al (2023) Plausible antioxidant and anticonvulsant potential of brain targeted naringenin-conjugated graphene oxide nanoparticles. *Biomass Convers Biorefinery*. <https://doi.org/10.1007/s13399-023-04343-1>
  27. Gopinath P, Jesu A, Manjunathan T, Ajay G (2021) 6-Gingerol and semisynthetic 6-Gingerdione counteract oxidative stress induced by ROS in zebrafish. *Chem Biodivers* 18:100374. <https://doi.org/10.1002/cbdv.202100650>
  28. Guru A, Murugan R, Arockiaraj J (2023) Histone acetyltransferases derived RW20 protects and promotes rapid clearance of *Pseudomonas aeruginosa* in zebrafish larvae. *Int Microbiol*. <https://doi.org/10.1007/s10123-023-00391-9>
  29. Murugan R, Rajesh R, Seenivasan B et al (2022) Withaferin A targets the membrane of *Pseudomonas aeruginosa* and mitigates the inflammation in zebrafish larvae; an in vitro and in vivo approach. *Microb Pathog* 172:105778. <https://doi.org/10.1016/j.micpath.2022.105778>
  30. Rudrappa M, Nayaka S, Kumar RS (2023) In Silico molecular docking approach of melanin against melanoma causing MITF proteins and anticancer, oxidation-reduction, photoprotection, and drug-binding affinity properties of extracted melanin from *Streptomyces* sp. strain MR28. *Appl Biochem Biotechnol* 195:4368–4386. <https://doi.org/10.1007/s12010-023-04358-4>
  31. Rudrappa M, Kumar RS, Basavarajappa DS et al (2023) *Penicillium citrinum* NP4 mediated production, extraction, physicochemical characterization of the melanin, and its anticancer, apoptotic, photoprotection properties. *Int J Biol Macromol* 245:125547. <https://doi.org/10.1016/j.ijbiomac.2023.125547>
  32. Sudhakaran G, Rajesh R, Murugan R et al (2022) Nimbin analog N2 alleviates high testosterone induced oxidative stress in CHO cells and alters the expression of Tox3 and Dennd1a signal transduction pathway involved in the PCOS zebrafish. *Phyther Res*. <https://doi.org/10.1002/ptr.7685>
  33. Guru A, Sudhakaran G, Almutairi MH et al (2022)  $\beta$ -cells regeneration by WL15 of cysteine and glycine-rich protein 2 which reduces alloxan induced  $\beta$ -cell dysfunction and oxidative stress through phosphoenolpyruvate carboxykinase and insulin pathway in zebrafish in-vivo larval model. *Mol Biol Rep*. <https://doi.org/10.1007/s11033-022-07882-4>
  34. Issac PK, Velayutham M, Guru A et al (2022) Protective effect of morin by targeting mitochondrial reactive oxygen species induced by hydrogen peroxide demonstrated at a molecular level in MDCK epithelial cells. *Mol Biol Rep* 49:4269–4279. <https://doi.org/10.1007/s11033-022-07261-z>
  35. N. Sai Supra AG, (2022) Pro-inflammatory cytokine molecules from *Boswellia serrate* suppresses lipopolysaccharides induced inflammation demonstrated in an in-vivo zebrafish larval model. *Mol Biol Rep* 49(8):7425–7435
  36. Livak KJ, Schmittgen TD (2001) Analysis of relative gene expression data using real-time quantitative PCR and the 2- $\Delta\Delta$ CT method. *Methods* 25:402–408. <https://doi.org/10.1006/meth.2001.1262>
  37. Heidari M, Doosti A (2023) *Staphylococcus aureus* enterotoxin type B (SEB) and alpha-toxin induced apoptosis in KB cell line.

- J Med Microbiol Infect Dis 11:96–102. <https://doi.org/10.52547/JoMMID.11.2.96>
38. Hong JM, Kim JE, Min SK et al (2021) Anti-Inflammatory effects of antarctic lichen *Umbilicaria antarctica* methanol extract in lipopolysaccharide-stimulated RAW 264.7 macrophage cells and zebrafish model. *Biomed Res Int* 2021:1–12. <https://doi.org/10.1155/2021/8812090>
39. Dhewang IB, Yudiati E, Subagiyo S, Alghazeer R (2023) Carrageenan extraction of *Kappaphycus alvarezii* seaweed from Nusa Lembongan waters using different alkaline treatments. *J Kelaut Trop* 26:238–244. <https://doi.org/10.14710/jkt.v26i2.17389>
40. Babapour H, Jalali H, Mohammadi Nafchi A (2021) The synergistic effects of zinc oxide nanoparticles and fennel essential oil on physicochemical, mechanical, and antibacterial properties of potato starch films. *Food Sci Nutr* 9:3893–3905. <https://doi.org/10.1002/fsn3.2371>
41. Doan Thi TU, Nguyen TT, Thi YD et al (2020) Green synthesis of ZnO nanoparticles using orange fruit peel extract for antibacterial activities. *RSC Adv* 10:23899–23907. <https://doi.org/10.1039/D0RA04926C>
42. Allaker RP (2012) The Use of Antimicrobial Nanoparticles to Control Oral Infections. *Nano-Antimicrobials*. Springer, Berlin, pp 395–425
43. Allaker RP, Memarzadeh K (2014) Nanoparticles and the control of oral infections. *Int J Antimicrob Agents* 43:95–104. <https://doi.org/10.1016/j.ijantimicag.2013.11.002>
44. Mendes CR, Dilarri G, Forsan CF et al (2022) Antibacterial action and target mechanisms of zinc oxide nanoparticles against bacterial pathogens. *Sci Rep* 12:1–10. <https://doi.org/10.1038/s41598-022-06657-y>
45. Rana N, Chand S, Gathania AK (2016) Green synthesis of zinc oxide nano-sized spherical particles using *Terminalia chebula* fruits extract for their photocatalytic applications. *Int Nano Lett* 6:91–98. <https://doi.org/10.1007/s40089-015-0171-6>
46. Brandelli A (2020) The interaction of nanostructured antimicrobials with biological systems: cellular uptake, trafficking and potential toxicity. *Food Sci Hum Wellness* 9:8–20. <https://doi.org/10.1016/j.fshw.2019.12.003>
47. Mi G, Shi D, Wang M, Webster TJ (2018) Reducing bacterial infections and biofilm formation using nanoparticles and nanostructured antibacterial surfaces. *Adv Healthc Mater* 7:1800103. <https://doi.org/10.1002/adhm.201800103>
48. Savage PB (2002) Design, synthesis and characterization of cationic peptide and steroid antibiotics. *Eur J Org Chem* 2002:759–768
49. Álvarez-Martínez FJ, Barraón-Catalán E, Herranz-López M, Micol V (2021) Antibacterial plant compounds, extracts and essential oils: an updated review on their effects and putative mechanisms of action. *Phytomedicine* 90:153626. <https://doi.org/10.1016/j.phymed.2021.153626>
50. Muñoz-Núñez C, Cuervo-Rodríguez R, Echeverría C et al (2023) Synthesis and characterization of thiazolium chitosan derivative with enhanced antimicrobial properties and its use as component of chitosan based films. *Carbohydr Polym* 302:120438. <https://doi.org/10.1016/j.carbpol.2022.120438>
51. Shanmugam K, Sarveswari HB, Udayashankar A et al (2020) Guardian genes ensuring subsistence of oral *Streptococcus mutans*. *Crit Rev Microbiol* 46:475–491. <https://doi.org/10.1080/1040841X.2020.1796579>
52. Elswaifi S, Palmieri J, Hockey K, Rzigalinski B (2009) Antioxidant nanoparticles for control of infectious disease. *Infect Disord - Drug Targets* 9:445–452. <https://doi.org/10.2174/187152609788922528>
53. Sathish M, Gobinath T, Sundaramanickam A et al (2022) Bio-medical applications of carrageenan hydrogel impregnated with zinc oxide nanoparticles. *Inorg Nano-Metal Chem* 52:734–745. <https://doi.org/10.1080/24701556.2021.1952243>
54. Motegi M, Takagi Y, Yonezawa H et al (2006) Assessment of genes associated with streptococcus mutans biofilm morphology. *Appl Environ Microbiol* 72:6277–6287. <https://doi.org/10.1128/AEM.00614-06>
55. Toledo-Arana A, Valle J, Solano C et al (2001) The enterococcal surface protein, Esp, is involved in enterococcus faecalis biofilm formation. *Appl Environ Microbiol* 67:4538–4545. <https://doi.org/10.1128/AEM.67.10.4538-4545.2001>
56. Yamazaki K, Kaneko Y, Suwa K et al (2005) Synthesis of potent and selective inhibitors of *Candida albicans* N-myristoyltransferase based on the benzothiazole structure. *Bioorg Med Chem* 13:2509–2522. <https://doi.org/10.1016/j.bmc.2005.01.033>
57. Markopoulos AK (2012) Current aspects on oral squamous cell carcinoma. *Open Dent J* 6:126–130. <https://doi.org/10.2174/1874210601206010126>
58. Zheng W, Zhou Q, Yuan C (2021) Nanoparticles for oral cancer diagnosis and therapy. *Bioinorg Chem Appl* 2021:1–14. <https://doi.org/10.1155/2021/9977131>
59. Luo M, Shao B, Nie W et al (2015) Antitumor and adjuvant activity of  $\lambda$ -carrageenan by Stimulating immune response in cancer immunotherapy. *Sci Rep* 5:11062. <https://doi.org/10.1038/srep11062>
60. Velayutham M, Sarkar P, Sudhakaran G et al (2022) Anti-cancer and anti-inflammatory activities of a short molecule, PS14 derived from the virulent cellulose binding domain of aphanomyces invadans, on human laryngeal epithelial cells and an in vivo Zebrafish embryo model. *Molecules* 27:7333. <https://doi.org/10.3390/molecules27217333>
61. Velayutham M, Sarkar P, Karupiah KM et al (2023) PS9, derived from an aquatic fungus virulent protein, glycosyl hydrolase, arrests MCF-7 proliferation by regulating intracellular reactive oxygen species and apoptotic pathways. *ACS Omega*. <https://doi.org/10.1021/acsomega.3c00336>

**Publisher's Note** Springer Nature remains neutral with regard to jurisdictional claims in published maps and institutional affiliations.

Springer Nature or its licensor (e.g. a society or other partner) holds exclusive rights to this article under a publishing agreement with the author(s) or other rightsholder(s); author self-archiving of the accepted manuscript version of this article is solely governed by the terms of such publishing agreement and applicable law.